Available online at www.sciencedirect.com
ScienceDirect
C. R. Physique 10 (2009) 548–559
COMPTES RENDUS PHYSIQUE
http://france.elsevier.com/direct/COMREN/

Theoretical spectroscopy / Spectroscopie théorique

Ab initio theory and calculations of X-ray spectra

John J. Rehr *, Joshua J. Kas, Micah P. Prange, Adam P. Sorini, Yoshinari Takimoto, Fernando Vila

Department of Physics, University of Washington, Seattle, WA 98195-1560, USA

Available online 5 December 2008

Abstract

There has been dramatic progress in recent years both in the calculation and interpretation of various x-ray spectroscopies. However, current theoretical calculations often use a number of simplified models to account for many-body effects, in lieu of first principles calculations. In an effort to overcome these limitations we describe in this article a number of recent advances in theory and in theoretical codes which offer the prospect of parameter free calculations that include the dominant many-body effects. These advances are based on *ab initio* calculations of the dielectric and vibrational response of a system. Calculations of the dielectric function over a broad spectrum yield system dependent self-energies and mean-free paths, as well as intrinsic losses due to multi-electron excitations. Calculations of the dynamical matrix yield vibrational damping in terms of multiple-scattering Debye–Waller factors. Our *ab initio* methods for determining these many-body effects have led to new, improved, and broadly applicable x-ray and electron spectroscopy codes. ***To cite this article: J.J. Rehr et al., C. R. Physique 10 (2009).***

Résumé

Théorie et calculs *ab initio* des spectres de rayons X. Ces dernières année ont vu des progrès spectaculaires tant dans le calcul que dans l'interprétation des différentes spectroscopies de rayons X. Cependant, pour tenir compte des effets à N corps, les calculs théoriques actuels utilisent souvent un certain nombre de modèles simplifiés, plutôt que les principes fondamentaux. Pour tenter de surmonter ces limitations, nous décrivons dans cet article plusieurs avancées récentes dans le domaine de la théorie et des codes informatiques, qui ouvrent la perspective de calculs sans paramètres incluant les effets dominants à N corps. Ces avances sont basées sur des calculs *ab initio* de la réponse diélectrique et vibrationelle d'un système. Des calculs de la fonction diélectrique sur une large gamme d'énergie fournissent, en fonction du système, les self-énergies et les libres parcours moyens, ainsi que les pertes intrinsèques dues aux excitations à plusieurs électrons. Des calculs de la matrice dynamique donnent l'amortissement vibrationel en fonction des facteurs de Debye–Waller à diffusion multiple. Nos méthodes *ab initio* pour la détermination des effets à N corps ont conduit à de nouveaux codes, améliorés et largement applicables, pour la spectroscopie des rayons X et des électrons. ***Pour citer cet article : J.J. Rehr et al., C. R. Physique 10 (2009).***

PACS: 78.70.Dm; 78.20.Ls; 75.50.Cc

Keywords: XAS; EXAFS; BSE; TDDFT

* Corresponding author.
E-mail address: jjr@phys.washington.edu (J.J. Rehr).

1631-0705/$ – see front matter
doi:10.1016/j.crhy.2008.08.004

1. Introduction

Significant progress has been made in recent years both in the theory and the interpretation of various x-ray spectroscopies. Our main aim in this chapter is to describe these advances, which are applicable to all spectroscopies involving electronic excitation, from x-ray absorption spectroscopy (XAS) [1], to x-ray Raman scattering (XRS) [2], to electron energy-loss spectroscopy (EELS) [3]. We begin by briefly reviewing the current status of these calculations, focusing primarily on the real-space Green's function (RSGF) approach [1]. This approach has been widely applied, especially to the extended x-ray absorption fine structure (EXAFS) and x-ray absorption near edge spectra (XANES) [4]. Schematically an x-ray absorption experiment measures the "x-ray absorption coefficient" $\mu(\omega)$, which characterizes the decay in intensity I of an x-ray beam passing through a material of thickness d, i.e., $I(d) = I_0 e^{-\mu(\omega)d}$. The absorption coefficient $\mu(\omega)$ is simply related to the imaginary part of the index of refraction $n(\omega)$ via $\mu(\omega) = 2(\omega/c)\,\mathrm{Im}\, n(\omega)$. By causality, which implies analyticity of optical response in the complex ω-plane, a full spectrum measurement of the absorption coefficient also determines the real part of the index of refraction. The terms EXAFS and XANES refer to the structure in the x-ray absorption spectrum $\mu(\omega)$ about 30 eV above and below the absorption edge energy, respectively. This energy scale is set by typical plasmon excitation energies ω_p, below which inelastic losses due to electronic excitations are relatively weak, leading to strong scattering. Although EXAFS is now fairly well understood [1], routine analysis of EXAFS experiments generally makes use of simplified models and a number of many-body parameters, e.g. Debye–Waller (DW) factors, mean free paths, and many-body amplitude factors. Similar considerations apply to XANES, where the agreement between theory and experiment is often less satisfactory. However, recent theoretical advances now offer the prospect of parameter free calculations of the spectra including many-body factors based on first principles calculations of dielectric and vibrational response.

Interestingly, the main idea behind our dielectric treatment of electron-electron interactions appears at first glance to be a "catch-22": the same information is contained in the dielectric function as in the absorption coefficient; so how can we begin to calculate a spectrum when the calculations require that we have already calculated the quantity that we are trying to calculate? The answer, of course, is that our dielectric approach is actually a "super self-consistency loop". The usefulness of this procedure relies on a good initial guess for the dielectric function, a good algorithm for generating the self-energy (a functional of the dielectric function), and the fact that this super self-consistency-loop converges adequately after only one iteration. Thus the strategy behind our approach is as follows: First, the RSGF approach is extended to permit calculations of dielectric response over a broad spectrum including the dominant low-energy region. From the dielectric response, we obtain system dependent self-energies and mean-free paths as well as intrinsic losses due to multi-electron excitations using GW and related methods [5]. Second, from first principles calculations of the dynamical matrix using auxiliary *ab initio* electronic structure codes and a Lanczos algorithm, we obtain vibrational damping in terms of multiple-scattering Debye–Waller factors. Together with advances in analysis, algorithms, and computer power, these developments have yielded improved calculations of both EXAFS and XANES as well as optical constants and x-ray scattering factors of large complex systems over a broad spectrum from the UV to x-ray energies.

2. Quasi-particle theory of XAS

The basic independent-particle theory of XAS is now well understood [1,6–9], and many current theoretical efforts are directed towards the first principles calculation and modeling of many-body effects. The contribution to the x-ray-absorption coefficient $\mu(\omega)$ at x-ray energy $\hbar\omega$ is proportional to the total absorption cross-section $\sigma(\omega)$. For a given material this cross-section can be calculated in terms of the many-body ground $|0\rangle$ and excited N-particle states $|F\rangle$ of the *embedded* atomic system, using Fermi's golden rule,

$$\sigma(\omega) = 4\pi^2 \frac{\omega}{c} \sum_F \left|\langle 0|d|F\rangle\right|^2 \delta(\omega + E_0 - E_F) \tag{1}$$

Here d is the coupling to the x-ray field, E_0 the ground-state energy, E_F excited-state energies, and we have used atomic units ($e = \hbar = m = 1$). Most practical calculations are based on the reduction of the many-body golden rule in Eq. (1) to an independent-electron approximation and a dipole approximation for the interaction $d = \hat{\epsilon} \cdot \mathbf{r}$. The sum over excited states F then reduces to a double-sum over "initial" (occupied) independent-electron states $|i\rangle$

and "final" (unoccupied) one-particle states $|f\rangle$. In this simple physical picture, the absorbed photon kicks a core-electron of energy E_i into a state above the Fermi-level (photoelectron state) of energy $E \equiv E_i + \omega$. The differences in various theoretical approaches reflect different approximations for the calculation of these ingredients. In particular, the question of precisely which independent-electron states to use is ambiguous and depends on the energy range of interest. One commonly used approach is based on the "final state rule," in which the independent-electron final states $|f\rangle$ are calculated in the presence of an appropriately screened core-hole. Theoretical justifications for these approximations have recently been developed [5,10] and also establish a close connection between the final state rule and Bethe–Salpeter Equation (BSE) calculations for deep-core spectra. An explicit calculation of the final states used in the independent-electron golden rule is often a computational bottleneck at high energies and can only be carried out efficiently for systems which are small or periodic. Even for periodic solids many single-particle approximations (including the final state rule) destroy periodicity due to the presence of a core-hole. Fortunately, explicit calculation of the final states can be avoided by re-expressing the XAS in terms of the retarded RSGF of the photoelectron,

$$G(E) = \frac{1}{E - h' + i\Gamma} = \sum_f |f\rangle \frac{1}{E - E_f + i\Gamma} \langle f| \tag{2}$$

Here $h' = p^2/2 + V'_{\rm Coul} + \Sigma(E)$, $V'_{\rm Coul}$ is the Coulomb potential which includes a screened core-hole, $\Sigma(E)$ is an energy-dependent self-energy, and Γ is the core-hole lifetime. In practice we have found that a self-consistently screened core-hole [1] gives a screened core-hole potential similar to that from linear response [11]. Clearly, the spectral representation of the Green's function, as given by the last term in Eq. (2), may be used to implicitly sum over final states. This significantly reduces the computational effort by eliminating the need for explicit calculations of the final state eigenfunctions. Thus the RSGF formalism greatly simplifies calculations of XAS for many applications, especially for complex, aperiodic systems. The approach also gives rise to a physical picture of the scattering processes in terms of a multiple scattering (MS) path expansion. In practice the RSGF method can only accommodate a finite cluster of atoms. However, this does not pose a limitation to the calculation of XAS, since inelastic losses limit the range probed by XAS experiment to the mean-free path λ. Since λ is typically between 5–20 Å for XAS, this corresponds to clusters of order 10^2 atoms about a given absorption site. This also explains why the quasi-particle theory of XAS is intrinsically a *short range order* theory.

The RSGF itself naturally separates into intra-atomic contributions from the central (absorbing) atom G^c and MS contributions from the environment G^{sc}. Thus $G = G^c + G^{sc}$, so that the XAS can be factored as $\mu = \mu_0(1 + \chi)$. As a result, the structure in μ depends to leading order on the "embedded" atomic background μ_0 (i.e., that defined by the solid-state potential at the absorption site) and on the *fine structure* χ due to MS from the environment. Within the RSGF approach it is generally convenient to represent G in an angular momentum $L = (\ell, m)$ basis about each atomic site in the sample. This yields the expression for the contribution to the XAS from a given core initial-state $|i\rangle$ at site R

$$\sigma(E) = 4\pi^2 \frac{\omega}{c} \sum_{L,L'} M^*_{L,i}(E) \rho_{L,L'}(E) M_{L',i}(E) \tag{3}$$

Here $M_{L,i}$ is the dipole matrix element between the core-state and a scattering-state $|L\rangle$ of angular momentum L, $\rho_{L,L'}(E) = -(1/\pi)\,\mathrm{Im}\, G_{L,L'}(E)$ is an element of the density-matrix at the absorbing atom, and for simplicity the site indices R and R' are suppressed. The scattering part of G may be expressed as a sum over all MS paths that a photoelectron can take away from the absorbing atom and back: first the photoelectron can scatter at any site in the sample, and second the scattering within an individual site R can be summed using a "site t-matrix". This yields a MS *path expansion* of the scattering contribution to the propagator

$$G^{sc}_{L,L'} = \left[\bar{G}^0 + \bar{G}^0 T \bar{G}^0 + \bar{G}^0 T \bar{G}^0 T \bar{G}^0 + \cdots\right]_{L,L'} \tag{4}$$

where the successive terms represent single, double, and higher order scattering processes. Typically, the maximum value of ℓ necessary for accurate EXAFS calculations using Eq. (4) is 25 or less for excitations up to about 1000 eV above threshold [12]. The T matrix has elements $T_{LR,L'R'} = t_{\ell R}\delta_{R,R'}\delta_{L,L'}$, where t includes all repeated scatterings within a given atomic cell. It is important to point out that in the above expression $\bar{G}^0$ refers to the damped free Green's function as calculated with a complex self-energy and core-hole lifetime, and subject to the condition that the site diagonal matrix elements $\bar{G}^0_{LR,L'R}$ are set to zero. At high energies the MS path expansion turns out to converge rapidly, typically with only of order 10^2 paths. This fast convergence is due to weakness of scattering (elements of

T small), and damping arising from the inelastic mean free path in the EXAFS energy regime (elements of G^0 for large $|R - R'|$ are small). Moreover, the MS expansion sometimes converges adequately in XANES, particularly for deep core-hole absorption in heavy elements which have short core-hole lifetimes. However, when the convergence is poor the MS expansion must be carried to very high or all orders (full MS), e.g., by explicit matrix inversion [13] or Lanczos algorithms [14], i.e.,

$$G^{\rm sc}_{L,L'} = \left[\left(1 - \bar{G}^0 T\right)^{-1} \bar{G}^0\right]_{L,L'} \tag{5}$$

The dimension of the matrix to be inverted in solving Eq. (5) is $N(\ell_{\rm max} + 1)^2$, where N is the number of atoms in the cluster and $\ell_{\rm max}$ is the maximum allowed angular momentum. For example, in a cluster of size 500 atoms in order to limit the matrix size to less than $10^4 \times 10^4$ one must limit the maximum ℓ value to 3 or less. Thus, since the maximum ℓ necessary for accurate calculations increases with distance from the edge, the FMS inversion is most useful for XANES calculations. The relativistic generalization of Eq. (5) is similar in form, the key formal difference being that the angular momenta are replaced with their relativistic generalization [15–17] $L \to (\kappa, m)$. Relativity is important for the treatment of spin-orbit coupling, which is large in the atomic core states and hence in transition matrix elements. On the other hand, relativity has only weak effects on the scattering and propagation of the photoelectron. In the FEFF8 multiple scattering (MS) code, these effects are treated to high accuracy using a relativistic Dirac–Fock approach [18] for atomic states and a semi-relativistic approximation for propagation.

The calculation of the scattering potentials to construct the site t-matrices simplifies for electrons at moderate energy (i.e., a few eV above threshold) where the scattering depends strongly only on the density in the core of an atom. In this deep core region, spherical symmetry of the potential is a good approximation. Self-consistent field (SCF) calculations of the potentials are nevertheless desirable even for EXAFS, since the Fermi energy threshold must be known to an accuracy better than a few eV for distance determinations better than 0.01 Å. In the SCF procedure in FEFF8, Coulomb potentials, electron densities, and the Fermi energy must be iterated typically about 10–20 times. As a result of hybridization and chemical bonding, the self-consistent atomic electron configurations in solids usually differ from those in atoms, and in general yield *fractional* average occupations of the various atomic levels. Comparisons with full-potential ground state electronic structure codes have shown that the spherical approximation is often valid for XAS, except within a few eV of threshold. Muffin-tin corrections can be important near threshold, especially in anisotropic systems. Thus, the development of efficient, full-potential RSGF approaches beyond the spherical muffin-tin approximation remains an important challenge for accurate XANES calculations [19].

Returning to the discussion of Eq. (4), we note that due to the large dimension of G, exact calculations with the path expansion can be carried out efficiently only for a few low-order MS paths [20]. To overcome this computational bottleneck, an efficient method based on the Rehr–Albers (RA) scattering matrix formalism [21] has been devised. The RA approach yields curved-wave calculations of the effective scattering amplitude $f_{\rm eff}(k)$ (from which the FEFF code takes its name) in terms of a separable representation of the free propagator $G^0(E)$. With this representation the MS expansion can be re-expressed as a sum over MS paths R in a form similar to the original EXAFS equation of Sayers, Stern and Lytle [22],

$$\chi(k) = S_0^2 \sum_R \frac{|f_{\rm eff}(k)|}{kR^2} \sin(2kR + \Phi_k) e^{-2R/\lambda_k} e^{-2\sigma^2 k^2} \tag{6}$$

An important difference, however, is the overall many-body amplitude factor S_0^2, reflecting the lack of orthogonality between initial and final states with and without the core-hole. Here $k = [2(E - E_F)]^{1/2}$ is the wavenumber measured from threshold E_F, $\lambda_k \approx k/(|\,\mathrm{Im}\,\Sigma| + \Gamma/2)$ is the XAFS mean-free path which is calculated in terms of the self-energy and core-hole lifetime Γ. Finally σ, which characterizes the thermal and structural disorder, is the rms fluctuation in the *effective path length* $R = R_{\rm path}/2$, which corresponds to peaks in the EXAFS Fourier transform. This equation has been automated in the FEFF codes and is now widely used to analyze EXAFS data. In addition, Eq. (6) illustrates the dominant many-body "inelastic parameters" S_0^2, λ_k and the vibrational DW factors σ^2, which we now show can be calculated from first principles.

3. Dielectric response and electronic inelastic losses

Theories of x-ray spectra and other "optical constants" have recently become increasingly sophisticated [1,23]. For example, treatments of such spectra can now go beyond the independent-particle approximation, e.g., with time-

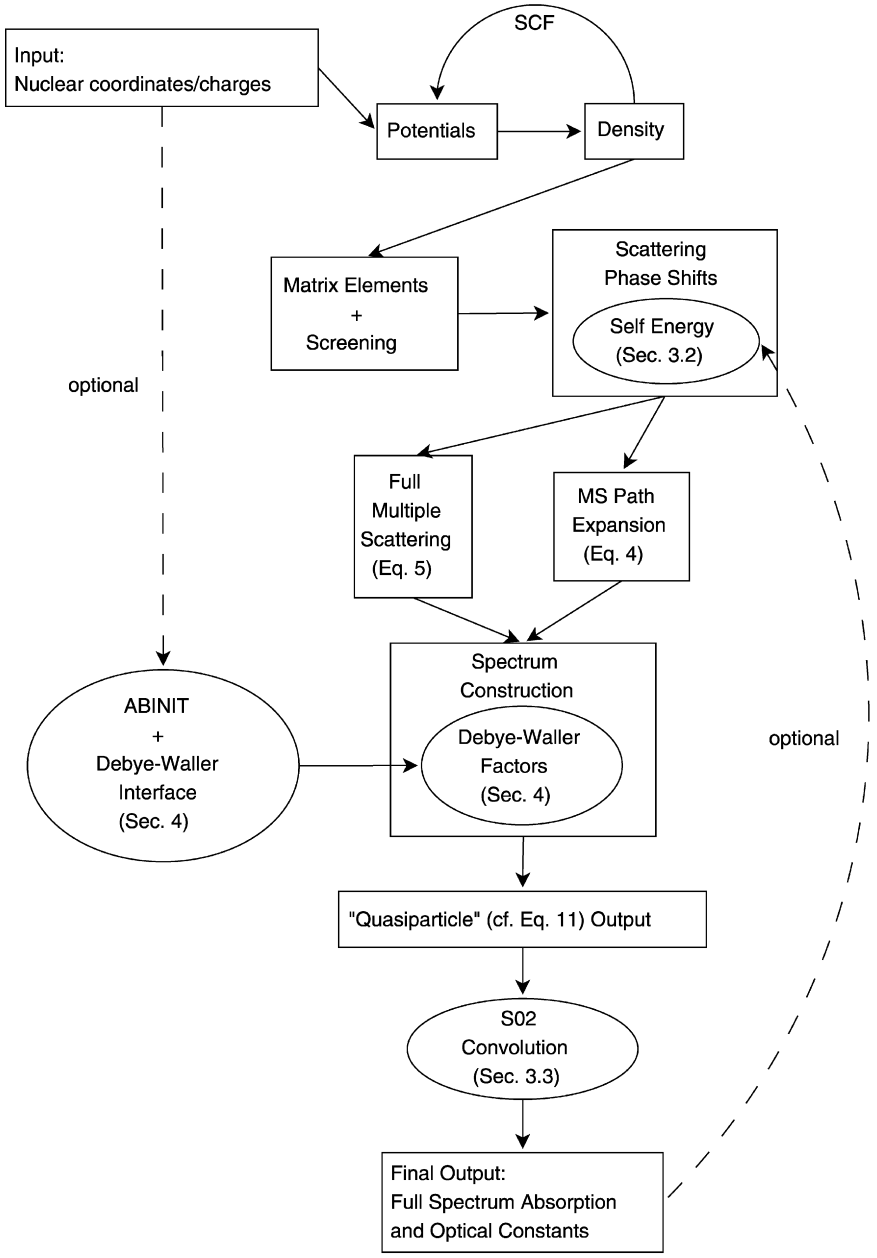

Fig. 1. Flow diagram for FEFF modules. New and improved modules which deal with inelastic losses are indicated by ellipses rather than boxes. The relevant sections and equations of this chapter regarding each improved module are indicated within parenthesis inside the ellipses.

dependent density functional theory (TDDFT) or the Bethe–Salpeter equation (BSE) [24,11]. However, less attention has been devoted to the effects of electronic inelastic losses at high energies. These losses are important both in spectroscopy and many other applications [25,26]. Moreover, current treatments [1,27,28] often utilize simplified or semi-empirical models with considerable variations in the results. To address these difficulties we present an approach for calculating the dielectric function using a RSGF formalism [1,11]. From a many-pole representation of the dielectric function and the GW approximation, we obtain photoelectron self-energies, inelastic mean free paths (IMFPs), and contributions from multi-electron excitations. By iterating these steps, we then obtain improved calculations of optical constants from the UV to x-ray energies. A flow diagram for the entire code is given in Fig. 1, and technical details are summarized below.

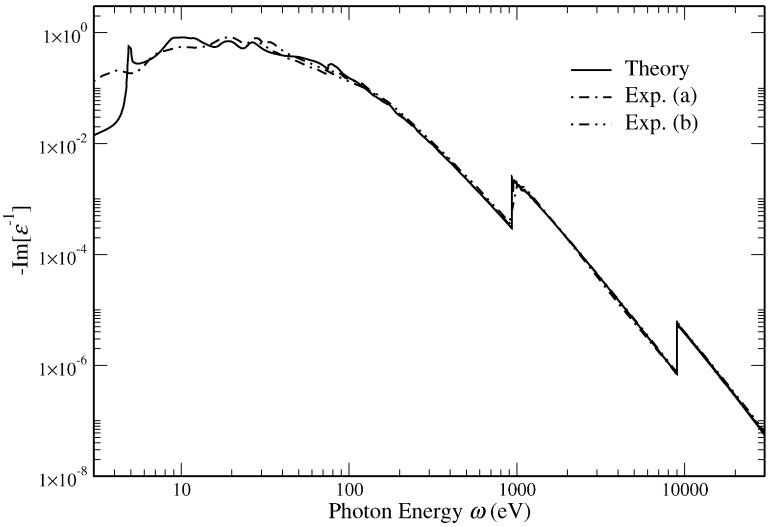

Fig. 2. Energy loss function $-\mathrm{Im}[\epsilon^{-1}]$ for fcc Cu *vs* photon energy ω as calculated using our approach [30] (solid), and from experiment (a) (dash-dot) [31] and (b) (dash-dot-dot) [32].

3.1. Dielectric function calculations in FEFF

A key physical quantity in these calculations is the position- and frequency-dependent complex susceptibility $\tilde{\chi}(\mathbf{r}, \mathbf{r}'; \omega)$ [23]. In the long wavelength limit, various optical constants are related to $\tilde{\chi}(\mathbf{r}, \mathbf{r}'; \omega)$ through the atomic polarizability $\alpha(\omega)$ [29],

$$\alpha(\omega) \equiv \int \mathrm{d}\mathbf{r}\, \mathrm{d}\mathbf{r}'\, d^{\dagger}(\mathbf{r})\, \tilde{\chi}(\mathbf{r}, \mathbf{r}'; \omega)\, d(\mathbf{r}') \tag{7}$$

where $d(\mathbf{r}) \equiv \hat{\epsilon} \cdot \mathbf{r}$ represents the dipole coupling to the photon field. Our RSGF approach for calculating $\alpha(\omega)$ [11] is summarized below, and also includes corrections to the independent particle approximation based on TDDFT following Ref. [29], and a screened core-hole for a given final state. Briefly, we first calculate the lossy part of the local embedded atom polarizability $\alpha(\omega)$, i.e.,

$$\mathrm{Im}\,\alpha(\omega) = \sum_{i,L,L'} \tilde{M}_{i,L} \big\langle \rho_{L,L'}(E) \big\rangle \tilde{M}_{L'i} \tag{8}$$

by summing the contributions from all occupied core states $|i\rangle$ of a given atom [30]. The real part $\mathrm{Re}\,\alpha(\omega)$ is then obtained from a Kramers transform. With TDDFT corrections, $\tilde{M}_{i,L}$ are *screened* dipole matrix elements between occupied core states $|i\rangle$ and final scattering states $|L\rangle$, in contrast to the bare dipole matrix elements of Eq. (3). The brackets $\langle \cdots \rangle$ denote a configurational average, which is expressed in terms of DW factors. For each core state $|i\rangle$, we first calculate the atomic-like background with no scattering; fine structure is then added with full MS to about 50 eV, and then with the MS path expansion to about 1500 eV above each edge. The screened dipole operators in $\tilde{M}_{L,i}$ account for the induced local fields [29]. From $\alpha(\omega)$ we obtain the dielectric constant $\epsilon(\omega) = 1 + 4\pi n \alpha(\omega)$, where $n = N/V$ is the atomic number density. For metals, the low-frequency behavior of $\epsilon(\omega)$ is approximated by an additive Drude term. Other optical constants, e.g., absorption coefficient μ, reflectivity R, anomalous x-ray scattering amplitudes $f_1 + if_2$, etc., are related to $\epsilon \equiv \epsilon_1 + i\epsilon_2$. Typical results [30], e.g., for the energy loss function $-\mathrm{Im}[\epsilon^{-1}] = \epsilon_2/[\epsilon_1^2 + \epsilon_2^2]$ for Cu (Fig. 2), are in reasonable agreement with experiment [31,32] from the UV and beyond. Additional examples are tabulated on the WWW [33].

3.2. Many-pole model self-energy

From the dielectric response, we can then obtain the self-energy $\Sigma(E)$ using Hedin's "GW approximation" [34],

$$\Sigma(E) = i \int \frac{\mathrm{d}\omega}{2\pi} G(E - \omega) W(\omega) e^{-i\delta\omega} \tag{9}$$

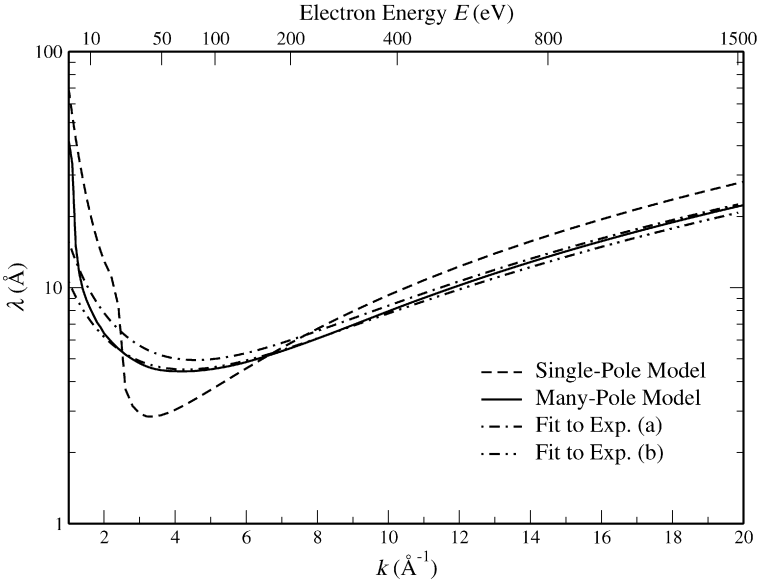

Fig. 3. Inelastic mean free path λ for fcc Cu *vs* electron wave number $k = (2E)^{1/2}$ and kinetic energy E for our many-pole model (solid), a single plasmon-pole model (dashes); and fits to experiment (dash-dots) (a) [39] and (b) [25].

where $W = \epsilon^{-1}(\omega)V$ is the screened coulomb interaction, and matrix indices $(\mathbf{r}, \mathbf{r}')$ are suppressed. For $G(E)$, we use the free Green's function, ignoring MS terms. Hence our $\Sigma(E)$ represents an *average* self-energy, which is adequate for calculations of spectral broadening. In contrast, current implementations for deep core spectra [1] have typically used a single plasmon-pole approximation for the dielectric function. Although computationally efficient, Fig. 2 shows that a single pole is not a good representation when the loss function has a broad spectrum. Thus, to obtain improved self-energies that exploit the efficiency of pole models, we match our *ab initio* $\epsilon(\omega)$ to a many-pole model, with poles spread over a sufficient spectral range,

$$-\mathrm{Im}\big[\epsilon^{-1}(\mathbf{q},\omega)\big] = \frac{\pi}{2}\sum_j g_j \omega_j \delta\big(\omega - \omega_j(\mathbf{q})\big) \tag{10}$$

where $g_j = (2\Delta\omega_j/\pi\omega_j)\mathrm{Im}[\epsilon^{-1}(\omega_j)]$ is the strength of pole j, and $\Delta\omega_j$ is the pole spacing. For simplicity, the momentum dependence of each pole is approximated by a polynomial in q^2: $\omega_j(\mathbf{q}) = [\omega_j^2 + v_F^2 q^2/3 + q^4/4]^{1/2}$ [35]. This approximation is roughly consistent with explicit calculations [2] and has the correct high q limit. The precise dispersion is not crucial, since $\mathbf{q}$ and ω are integrated over [35]. Many-pole models [36] and other methods [37] have been developed previously for more accurate self-energy calculations; however, they are computationally demanding and not applicable at high photoelectron energies, e.g., for EXAFS. Our model is similar to that of Ref. [27], but does not rely on empirical optical constants. Our algorithm for the many-pole dielectric function of Eq. (10) is key to an efficient calculation of the many-body effects in core-level XAS [38], and should be widely applicable.

Using our many-pole model in the GW approximation of Eq. (9), we can obtain an efficient approximation for the self-energy as a sum over single-pole models $\Sigma_1(E;\omega_j)$ with excitation energies ω_j, i.e., $\Sigma(E) = \sum_j g_j\ \Sigma_1(E,\omega_j)$. As a check, we have calculated the IMFP $\lambda = (E/2)^{1/2}/|\,\mathrm{Im}\,\Sigma(E)|$ for various materials [33]. Fig. 3 shows λ for fcc Cu using a 100-pole model matched to the loss function in Fig. 2. Clearly this model corrects the excessive loss of the single-pole model below 100 eV, and yields quantitative agreement with fits to experiment [25,39]. Our self-energy is also in reasonable agreement with that of Ref. [36]. Similar approaches [40] can be applied to calculations of stopping powers in inelastic electron scattering [26], and to photoemission spectra [28].

3.3. Satellite excitations

Our many-pole model in Eq. (10) also permits calculations of inelastic losses due to multi-electron (e.g. "shake-up" and "shake-off") excitations. These can be calculated using a generalization of the GW approximation and a quasi-

boson model, as described in detail in Ref. [5]. Such excitations correspond to satellites beyond the quasi-particle peak in the spectral function $A = (-1/\pi)\,\mathrm{Im}\,G_{\mathrm{eff}}$, where G_{eff} is an effective one-particle propagator. In addition to intrinsic losses, G_{eff} contains energy-dependent interference terms, which tend to suppress the satellites. The net effect can be included in the x-ray absorption $\mu(\omega)$ in terms of a convolution of a normalized spectral function $\tilde{A}$ and the quasi-particle absorption coefficient μ_{qp}, which ignores satellites,

$$\mu(\omega) = \int_0^\infty \mathrm{d}\omega'\, \tilde{A}(\omega,\omega')\mu_{qp}(\omega-\omega') \equiv \big\langle \mu_{qp}(\omega)\big\rangle \tag{11}$$

where ω' is the excitation energy [5]. Likewise, the net EXAFS is given by a convolution of $\tilde{A}$ with the quasi-particle fine structure. For each MS path R, the convolution over the fine structure yields an amplitude reduction factor $S_R^2(\omega)$ and (since $\tilde{A}$ is asymmetric) a negative phase shift $\Delta_R(\omega)$, $\langle e^{2ikR}\rangle = S_R^2(\omega)e^{2ikR+\Delta_R(\omega)}$. For example, for the first shell of Cu, we find that $S_R^2(\omega)$ and $\Delta_R(\omega)$ cross-over smoothly from the adiabatic (or quasi-particle) limit at threshold to nearly constant values $S_0^2 \approx 0.92$ and $\Delta_R \approx -0.2$ rad in the EXAFS. This behavior is roughly consistent with experiment $S_R^2 \approx 0.9$ [5].

4. Debye–Waller factors and vibrational damping

As noted above, quantitative analysis of EXAFS spectra requires the knowledge of DW factors arising from thermal vibrations and structural disorder. These factors are an essential component of Eq. (6), resulting from the thermal and configurational average $\langle\mu(E)\rangle$ of the x-ray absorption coefficient $\mu(E)$ over the pair (or MS path length) distribution function. The vibrational and structural disorder effects are additive, but since the latter depend on external factors like sample history and preparation, presently we will only focus on the vibrational contribution. The DW factors vary as $\exp[-W(T)]$, where $W(T) \approx 2k^2\sigma^2(T)$, and $\sigma^2(T) = \langle[(\mathbf{u}_R - \mathbf{u}_0)\cdot\hat{\mathbf{R}}]^2\rangle$ is the mean square relative displacement (MSRD) of a given MS path [41]. This causes damping of the spectra with respect to increasing temperature T and wave number k. The thermal effects on the normalized EXAFS spectrum $\chi(k)$ are dominated by the average over the oscillatory behavior $\langle\chi_R(k)\rangle \propto \langle\sin(2kR+\Phi)\rangle$ of each path of length R in the MS path expansion. Thus these DW factors, which depend only on the path-length distribution function, apply to related spectroscopies which can be described by a MS path expansion. The XAFS DW factor is also analogous to those arising in x-ray and neutron diffraction, where $W(T) = (1/2)k^2u^2(T)$, and $u^2(T) = \langle(\mathbf{u}\cdot\hat{\mathbf{R}})^2\rangle$ is the mean-square atomic displacement.

The thermal averages described above are given by Debye integrals over the vibrational density of states (VDOS) $\rho_R(\omega)$ projected onto a given MS path R [42–44]:

$$\sigma_R^2(T) = \frac{\hbar}{2\mu}\int_0^\infty \frac{1}{\omega}\coth\left(\frac{\beta\hbar\omega}{2}\right)\rho_R(\omega)\,\mathrm{d}\omega. \tag{12}$$

Here μ is the reduced mass associated with the path R, and $\beta = 1/k_BT$. Heretofore, these DW factors have been estimated using semiempirical Einstein or Debye models [45,46] or fitted to experimental data. Although these methods are quite useful, they are not completely satisfactory for several reasons: (i) the available experimental data only allows reliable fits to a few parameters; (ii) semiempirical models require different Debye or Einstein temperatures for different MS paths; and (iii) such models do not capture the anisotropic structure of the phonon spectra [47,42]. However, we have found that these limitations can largely be surmounted when the VDOS is calculated using a continued fraction representation of the lattice dynamical Green's function (LDGF), generated with the iterative Lanczos algorithm [48]. From the imaginary part of the LDGF we have [42,43]:

$$\rho_R(\omega) = -\frac{2\omega}{\pi}\mathrm{Im}\left\langle Q_R\left|\frac{1}{\omega^2-\mathbf{D}+i\epsilon}\right|Q_R\right\rangle \tag{13}$$

where $|Q_R\rangle$ is a Lanczos seed state representing a normalized, mass-weighted displacement of the atoms along the path R, and $\mathbf{D}$ is the dynamical matrix of force constants. If a different seed displacement is used, for instance an

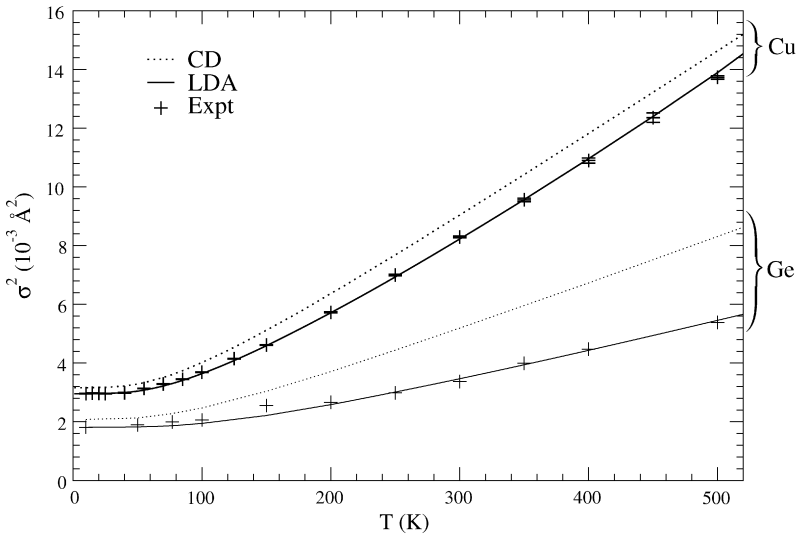

Fig. 4. Temperature dependence of the Debye–Waller factor for the nearest neighbor single scattering path in Cu and Ge. The experimental difference values (from [54] for Cu and [55] for Ge) were shifted to match the LDA results at 0 K.

atomic shift or a shift orthogonal to a path, different projections of the VDOS can be obtained [49]. Here **D** is defined as

$$D_{jl\alpha,j'l'\beta} = (M_j M_{j'})^{-1/2} \frac{\partial^2 E}{\partial u_{jl\alpha} \partial u_{j'l'\beta}} \tag{14}$$

where $u_{jl\alpha}$ is the $\alpha = \{x, y, z\}$ Cartesian displacement from the equilibrium position of atom j in unit cell l, M_j is the mass of atom j, and E is the total internal energy of the system. Within this formulation, the problem is reduced to finding an accurate model for **D**. Empirical estimates of the interatomic force constants are sometimes available, but their temperature dependence limits their accuracy and generality. Alternatively, first principles electronic structure methods can now be used to determine **D** with sufficient accuracy for both periodic and molecular systems [50–52]. For crystalline systems **D** can be obtained e.g., using ABINIT [53]. Fig. 4 shows typical results for Cu and Ge, obtained with the local density approximation (LDA) [56,49] and, for comparison, the correlated Debye (CD) model. While the LDA results are in good agreement with experiment [54,55], the CD model [1] works well for Cu but gives significant errors for the more anisotropic Ge. Finally, the main effects of anharmonicity can be included by calculating the dynamical matrix for equilibrium positions corresponding to a temperature-dependent lattice constant $a(T)$ [49]. This method yields the net thermal expansion $\Delta a = a(T) - a_0$. Also, including the perpendicular component of the expansion $\sigma_\perp^{(1)} = \langle |\Delta \mathbf{u}_\perp|^2 \rangle / (2R_0)$, it yields the first EXAFS cumulant. For instance, for Cu at 300 K, the first cumulant is 0.0217 Å in good agreement with the experimental value 0.0205 ± 0.0009 Å [54]. Estimates for the third cumulant are obtained using cumulant relations [49].

5. Results and conclusions

Calculations based on the standard quasiparticle theory and the RSGF formalism now make possible a general treatment of XAS, encompassing XANES and EXAFS, as well as a number of other x-ray spectroscopies. These calculations typically rely on simplified models to deal with many-body effects. However, recent theoretical advances have led to efficient, *ab initio* approaches for calculations of the key many-body damping factors in these core-level x-ray spectroscopies.

In summary, our calculations of these many-body effects are made possible by three key developments: (i) an extension of our RSGF code for full-spectrum calculations; (ii) an efficient many-pole representation of the dielectric function; and (iii) an efficient Lanczos approach for phonon spectra and DW factors. These developments yield significantly improved self-energies compared to plasmon-pole models, as well as quantitative IMFPs and losses due to multi-electron excitations. All of these many-body effects are important in calculations of optical constants over

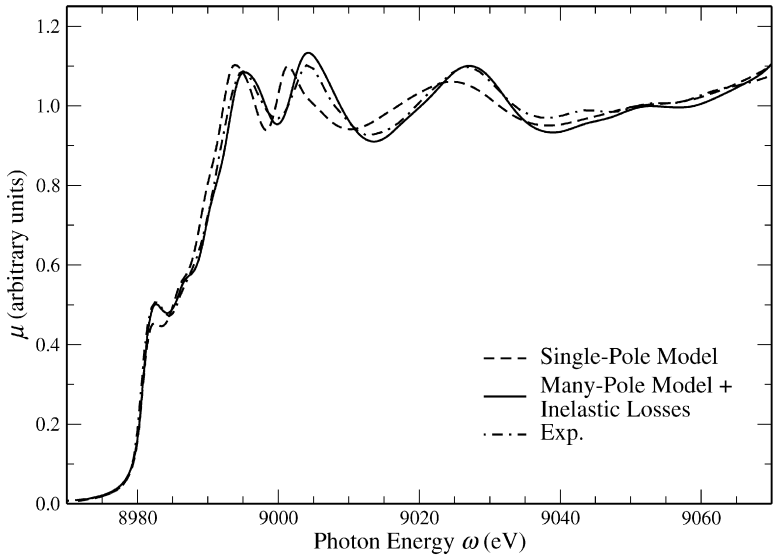

Fig. 5. X-ray absorption μ *vs* photon energy ω for fcc Cu for our many-pole model with inelastic losses (solid); a single-pole model (dashes); and experiment (dash-dots) [57].

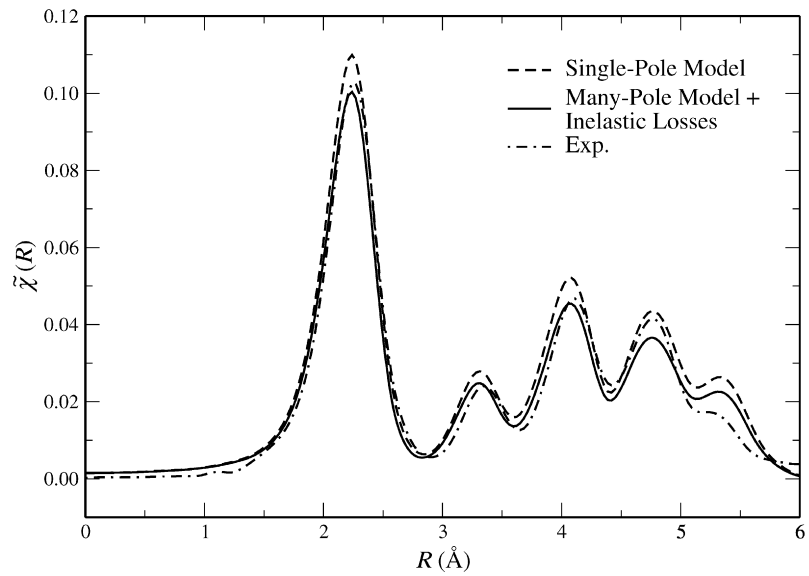

Fig. 6. Fourier transform of the Cu K-edge EXAFS $\tilde{\chi}(R)$ at 10K vs half MS path-length R with (solid), and without inelastic losses (dashes), and from experiment (dash-dots) [57].

a broad spectrum, and their inclusion yields improved amplitudes and phases from the UV to x-ray energies [33]. The results presented show that the new approaches for calculating inelastic losses, self-energies, and Debye–Waller factors yield significant improvements in amplitude and phase compared to the semi-empirical approaches, both for the near edge spectra (XANES) (Fig. 5) and the EXAFS (Fig. 6). Our approach includes solid state effects (e.g., edge shifts, fine structure, and temperature dependent DW factors) and is applicable to general aperiodic materials. Thus our optical constants complement and can potentially replace empirical tables [31,32,58–60] or atomic models [61] for many applications. Extensions, e.g, to spectra at finite momentum transfer and to the visible regime with improved potentials are also possible [2].

Acknowledgements

We gratefully acknowledge the contributions to this work by our colleagues, in particular R.C. Albers, A.L. Ankudinov, L.W. Campbell, Z.H. Levine, G. Putzel, J.A. Soininen, and E.L. Shirley. This work is supported in part by the DOE Grant DE-FG03-97ER45623 (JJR, MPP) and DE-FG02-04ER1599 (FDV), NIH NCRR BTP Grant RR-01209 (JJK), NIST Grant 70 NAMB 2H003 (APS), NSF Grant 0120967 (YT), and was facilitated by the DOE Computational Materials Science Network.

References

[1] J.J. Rehr, R.C. Albers, Rev. Mod. Phys. 72 (2000) 621.
[2] J.A. Soininen, A.L. Ankudinov, J.J. Rehr, Phys. Rev. B 72 (2005) 045136.
[3] M.S. Moreno, K. Jorissen, J.J. Rehr, Micron 38 (2007) 1.
[4] A.L. Ankudinov, et al., Phys. Rev. B 58 (1998) 7565.
[5] L.W. Campbell, et al., Phys. Rev. B 65 (2002) 064107.
[6] P.A. Lee, J.B. Pendry, Phys. Rev. B 11 (1975) 2795.
[7] W.L. Schaich, Phys. Rev. B 8 (1973) 4028.
[8] C.R. Natoli, et al., Phys. Rev. A 22 (1980) 1104.
[9] T. Fujikawa, N. Yiwata, Surf. Sci. 358 (1996) 60.
[10] J.J. Rehr, J.A. Soininen, E.L. Shirley, Phys. Scripta T 115 (2005) 207.
[11] A.L. Ankudinov, Y. Takimoto, J.J. Rehr, Phys. Rev. B 71 (2005) 165110.
[12] A.L. Ankoudinov, Relativistic spin-dependent X-ray absorption theory, PhD thesis, University of Washington, 1996.
[13] P.J.H.C. Durham, P.J., Comput. Phys. Commun. 25 (1982) 193.
[14] A.L. Ankudinov, et al., Phys. Rev. B 65 (2002) 104107.
[15] H. Ebert, Rep. Prog. Phys. 59 (1996) 1665.
[16] A. Messiah, Quantum Mechanics, John Wiley & Sons, Inc., New York, 1962.
[17] I.P. Grant, Adv. Phys. 19 (1970) 747.
[18] Z.S. Ankudinov, A.L.J. Rehr, Comput. Phys. Commun. 98 (1996) 359.
[19] A.L. Ankudinov, J.J. Rehr, Phys. Scripta T 115 (2005) 24.
[20] N.B.S.J. Gurman, I. Ross, J. Phys. C: Solid State 19 (1986) 1845.
[21] J.J. Rehr, R.C. Albers, Phys. Rev. B 41 (1990) 8139.
[22] D.E. Sayers, E.A. Stern, F.W. Lytle, Phys. Rev. Lett. 27 (1971) 1204.
[23] G. Onida, L. Reining, A. Rubio, Rev. Mod. Phys. 74 (2002) 601.
[24] J.A. Soininen, E.L. Shirley, Phys. Rev. B 64 (2001) 165112.
[25] C.J. Powell, A. Jablonski, J. Phys. Chem. Ref. Data 28 (1999) 19.
[26] J.M. Fernandez-Varea, et al., Nucl. Instrum. Methods Phys. Res., Sect. B 229 (2005) 187.
[27] W. von der Linden, P. Horsch, Phys. Rev. B 37 (1988) 8351.
[28] E.E. Krasovskii, et al., Phys. Rev. B 66 (2002) 235403.
[29] A. Zangwill, P. Soven, Phys. Rev. A 21 (1980) 1561.
[30] M.P. Prange et al., unpublished.
[31] H.J. Hagemann, W. Gudat, C. Kunz, J. Opt. Soc. Am. 65 (1975) 742.
[32] B.L. Henke, E.M. Gullikson, J.C. Davis, Atom. Data Nucl. Data 54 (1993) 181.
[33] M.P. Prange, G. Rivas, J.J. Rehr, Tables of Optical Constants, WWW, http://leonardo.phys.washington.edu/feff/opcons/, 2005.
[34] L. Hedin, S. Lundqvist, Solid State Phys. 23 (1969) 1.
[35] B. Lundqvist, Phys. Kondens. Mater. 6 (1967) 193.
[36] J.A. Soininen, J.J. Rehr, E.L. Shirley, J. Phys.: Condens. Mat. 15 (2003) 2572.
[37] I. Campillo, et al., Phys. Rev. Lett. 83 (1999) 2230.
[38] J.J. Kas, et al., Phys. Rev. B 76 (2007) 195116.
[39] C.M. Kwei, et al., Surf. Sci. 293 (1993) 202.
[40] A.P. Sorini, et al., Phys. Rev. B 74 (2006) 165111.
[41] E.D. Crozier, J.J. Rehr, R. Ingalls, in: D.C. Koningsberger, R. Prins (Eds.), X-Ray Absorption: Principles, Applications, Techniques of EXAFS, SEXAFS, and XANES, Wiley, New York, 1988, p. 375.
[42] A. Poiarkova, J.J. Rehr, Phys. Rev. B 59 (1999) 948.
[43] A. Poiarkova, J.J. Rehr, J. Synchrotron Radiat. 8 (2001) 313.
[44] H.J. Krappe, H.H. Rossner, Phys. Rev. B 66 (2002) 184303.
[45] E. Sevillano, H. Meuth, J.J. Rehr, Phys. Rev. B 20 (1979) 4908.
[46] N. Van Hung, J.J. Rehr, Phys. Rev. B 56 (1997) 43.
[47] N. Dimakis, G. Bunker, Phys. Rev. B 58 (1998) 2467.
[48] P. Deuflhard, A. Hohmann, Numerical Analysis, de Gruyter, Berlin, 1995.
[49] F.D. Vila, et al., Phys. Rev. B 76 (2007) 014301.

[50] S. Baroni, et al., Rev. Mod. Phys. 73 (2001) 515.
[51] C. Lee, X. Gonze, Phys. Rev. B 51 (1995) 8610.
[52] G.M. Rignanese, J.P. Michenaud, X. Gonze, Phys. Rev. B 53 (1996) 4488.
[53] X. Gonze, et al., Comp. Mat. Sci. 25 (2002) 478.
[54] P. Fornasini, et al., Phys. Rev. B 70 (2004) 174301.
[55] G. Dalba, et al., Phys. Rev. Lett. 82 (1999) 4240.
[56] J.P. Perdew, Y. Wang, Phys. Rev. B 45 (1992) 13244.
[57] M. Newville, Thermal Expansion in EXAFS, PhD thesis, University of Washington, 1994.
[58] E.D. Palik (Ed.), Handbook of Optical Constants of Solids, Academic Press, Orlando, 1985.
[59] C.T. Chantler, J. Phys. Chem. Ref. Data 24 (1995) 71.
[60] W.T. Elam, B.D. Ravel, J.R. Sieber, Rad. Phys. Chem. 63 (2002) 121.
[61] D. Liberman, J.T. Waber, D.T. Cromer, Phys. Rev. 137 (1965) A27.